Investigating the impact of atrial fibrillation on the vascular onset of glaucoma via multiscale cardiovascular modeling

Investigating the impact of atrial fibrillation on the vascular onset of glaucoma via multiscale cardiovascular modeling

Stefania Scarsoglio[a,b,*], Luca Congiu[a], Luca Ridolfi[c,b]

[a]*Department of Mechanical and Aerospace Engineering, Politecnico di Torino, Corso Duca degli Abruzzi 24, Turin, (10129), Italy*
[b]*PolitoBioMed Lab, Politecnico di Torino, Corso Duca degli Abruzzi 24, Turin, (10129), Italy*
[c]*Department of Environmental, Land and Infrastructure Engineering, Politecnico di Torino, Corso Duca degli Abruzzi 24, Turin, (10129), Italy*

Abstract

Background and objective: Atrial fibrillation (AF) is the most common tachyarrhythmia, exhibiting faster and irregular beating. Although there is growing evidence of the impact of AF on the cerebral hemodynamics, ocular hemodynamic alterations induced by AF are still poorly investigated to date. The objective of this study is to computationally inquire into the role of AF on the ocular hemodynamics as one of the possible vascular triggers of glaucoma, which is the leading cause of blindness due to the damage of the optic nerve.
Methods: A validated 0D-1D multiscale cardiovascular model is exploited to compute the hemodynamic response of AF against sinus rhythm (SR), by simulating 2000 beats for each condition. To mimic AF rhythm, its main features are accounted for: (i) accelerated, variable and uncorrelated beating; (ii) absence of atrial kick; (iii) ventricular systolic dysfunction.
Results: We focused on intraocular pressure (IOP), ocular perfusion pressure (OPP), and translaminar pressure (TLP). Apart from a modest OPP decrease, beat-averaged values of IOP and TLP barely vary in AF with respect to SR. Instead, during AF a significant reduction and dispersion of pulsatile values (i.e., maximum minus minimum values reached in a beat),

*Corresponding author: stefania.scarsoglio@polito.it

as well as wave amplitude damping, is observed for IOP, OPP and TLP. The marked variabiliy of pulsatile values, which are hardly measured due to clinical difficulties, can induce transient hypoperfusions and hypo-pulsatility events (for OPP) as well as hypertensive episodes (for TLP).
Conclusions: Awaiting necessary clinical data which are to date lacking, the present study can enrich - through hemodynamic-driven hints in the AF framework - the vascular theory, which associates reduced ocular perfusion (by means of decreased OPP and increased TLP) to an augmented risk of glaucoma. In this context, present modeling findings suggest a possible mechanistic link between AF-induced hemodynamic alterations and the increased risk of glaucoma development.

Keywords: atrial fibrillation, intraocular pressure, computational hemodynamics, glaucoma, cardiovascular multiscale modeling, ocular perfusion pressure, translaminar pressure

1. Introduction

Atrial fibrillation (AF), characterized by a faster and irregular heart beating, is the most common cardiac arrythmia and currently affects about 60 million subjects worldwide [1]. Due to the increasing life expectancy in Western countries, its incidence is expected to more than double within the next forty years [2]. Beside disabling symptoms - such as palpitations, chest discomfort and reduced exercise tolerance - there is growing evidence that AF is associated to cognitive decline, independently from clinical strokes [3, 4]. The alteration of cerebral hemodynamics during AF is extremely promising, though one of the least investigated mechanisms possibly relating AF and cognitive decline [4, 5]. Driven by the recent attention regarding the AF impact on the cerebral hemodynamics and considering that cerebral and ocular hemodynamics are intrinsically related through the retrobulbar subarachnoid space which is governed by the intracranial pressure (ICP), we here aim at investigating the acute response of ocular hemodynamics to AF events. In particular, we inquire into the role that AF-induced hemodynamics may play in the development of glaucoma.

Glaucoma is the leading cause of blindness due to the damage of the optic nerve, with 80 million people affected worldwide [6]. Although an increased intraocular pressure (IOP) is believed to be a major risk factor and the main trigger mechanism for glaucoma [6, 7], the underlying mechanisms are

debated. According to the vascular theory, two parameters defined through IOP - namely the ocular perfusion pressure, $OPP = Pa_{eye} - IOP$ (where Pa_{eye} is the arterial pressure at the eye level), and the translaminar pressure, $TLP = IOP - ICP$ - play a key role. In particular, a decreased OPP and an increased TLP are potential markers associated with the increased risk of glaucoma development [7–9]. However, existing literature investigating the link between OPP and glaucoma is divided, as in subjects with glaucoma mean OPP is found to increase [10–12], remain equal [13–15], and reduce [16–18], with respect to the control population. Thus, definitive findings either confirming or refuting vascular theory are still missing.

In vivo measurements investigating the role of AF on the ocular hemodynamics and the development of glaucoma are even more contrasting, also considering the very few number of studies. A significant association between AF and glaucoma development was found [19, 20], even if results on IOP are not definitive, showing a modest increase [21], but also a reduction [22]. In this context of lack of clinical data, the adoption of a cardiovascular modeling framework can be greatly valuable to shed light on the hemodynamic mechanisms induced by AF able to alter IOP. Although not focused on the AF-ocular hemodynamics link, a number of computational approaches have been in fact successfully proposed to investigate the cardiovascular response in presence of cardiac arrhythmias, by focusing on the cerebral [23–28], cardiac-coronary [29–32], valvular [33, 34], and arterial [35–37] hemodynamics, as well as the thromboembolic risk in the left atrial appendage [38–40].

We here propose a 0D-1D multiscale cardiovascular model - previously exploited and validated in different pathological [29, 30, 35, 41] and altered gravity [42–46] conditions – to study the AF effects on the ocular hemodynamics and thus contribute to understand the possible vascular link between AF and glaucoma. The model combines a 1D description of the arterial tree and coronary circulation, with a 0D representation of the distal circulation, venous return, cardiopulmonary and cerebro-ocular circulations. The overall model is equipped with baroreflex and cardiopulmonary regulation mechanisms, as well as cerebral autoregulation, and explicitly accounts for posture and gravity changes. Through a stochastic modeling, we aim at investigating the impact of acute AF on the ocular hemodynamics variables with respect to the sinus rhythm (SR). We considered two representative configurations of SR and AF rhythms imposed on a generic healthy young patient in supine posture, by simulating for each condition 2000 beats to guarantee the statistical significance of the outcomes. SR was simulated at the typical resting

HR (mean 70 bpm) with Gaussian distributed and time-correlated regular beats. AF configuration instead accounted for the most important AF features: (i) accelerated, variable and uncorrelated beating (mean 90 bpm), extracted from an exponentially-modified Gaussian distribution; (ii) absence of atrial kick; (iii) ventricular systolic dysfunction (i. e., reduced left and right ventricular contraction) [31, 32, 36]. After validating the model by means of typical central cardiovascular parameters - such as stroke volume, cardiac output and mean arterial pressure – we focused on significant ocular circulation parameters, IOP, OPP and TLP. The comparison between SR and AF allowed us to quantify the net hemodynamic impact of AF on the ocular compartment and inquire into its possible mechanistic role in the development of glaucoma.

2. Methods

The present study was conducted exploiting a 0D-1D multiscale closed-loop model of the cardiovascular system. The model has been recently and extensively validated against posture [43, 46, 47] and gravity [42, 44, 45] changes, as well as in AF conditions [29, 30, 35]. The present modeling approach allowed to obtain a reliable description of several characteristics of the cardiovascular system and currently comprises a 1D representation of the systemic arterial and coronary circulations linked to several 0D lumped parameter compartments that describe the peripheral, venous, cardiopulmonary, and cerebral-ocular circulations. In the next sections, we will recall the most relevant features of the whole model, by focusing on the ocular compartment. Complete modeling details are offered in the Supplementary Material. Then, the stochastic approach to simulate SR and AF is presented, paying attention to the hemodynamic features characterizing AF rhythm.

2.1. Cardiovascular modeling

The 1D model consists of 63 main large arteries, which are described as straight tapered vessels, with a circular cross-sectional shape. The blood motion is described by one-dimensional mass and momentum conservation equations, where the cross-section area $A(x,t)$ and the flow $Q(x,t)$ are the dependent variables, being x and t the axial space coordinate and the time, respectively. At each inlet/outlet, mass and momentum conservation are set as boundary condition. A constitutive equation, linking $P(x,t)$ and $A(x,t)$, is introduced to describe the non-linear mechanical behavior of the large

arteries. The blood is modeled as a Newtonian fluid with density $\rho = 1050$ kg/m^3.

The 1D model is connected to the 0D peripheral circulation compartments, each described by an electric analog circuit. The terminal branches of the main arteries interface with the arteriolar vessels, which are modelled using characteristic impedances, Z_c. Downstream the arteriolar compartments, the terminal of the coronary arteries is connected to a lumped model of the coronary microcirculation bed, which provides a distinctive identification of the vasculature perfusing each myocardial layer - from the subepicardial, through the intermediate midwall, up to the subendocardial circulation - each described into arterial, intermediate, and venous subcompartments. The internal carotid and the vertebral arteries are linked to a 0D cerebro-ocular model, which starts with a lumped representation of the main large cerebral arteries of the circle of Willis. Then, six branches extend from the circle of Willis to supply the right and left pial circulation. The pial circulation is followed by the intracerebral arteriolar circulation, which is further subdivided into anterior, middle, and posterior circulation, interconnected through collateral vessels. Ultimately, the intracerebral arteriolar circulation merges into one capillary-venous compartment that, along with the ocular circulation, connects to the superior vena cava.
The remaining terminal branches other than coronary and cerebral arterioles merge into five macro-regions that describe the microcirculation of legs, lower abdomen, upper abdomen, arms, and head. Each of the five macro-regions is divided into three compartments, representing the capillary, venule, and vein circulations. The leg and arm venous compartments include a model of the venous valve that prevents the reversal flow. Finally, three compartments conclude the venous return with the abdominal, inferior, and superior venae cavae, the latter including a venous collapse mechanism. Additional lumped parametrizations are adopted for the four cardiac chambers and valves, and the pulmonary circulation. The cardiac contractility is modeled employing time-varying elastances, one specific for the atria and one for the ventricles. The four cardiac valves are represented by four non-ideal diodes, accounting for various factors affecting the valve leaflets such as tissue friction, pressure and inertial forces, and the influence of downstream vortexes.

The model is equipped with short-term regulation mechanisms, accounting for the baroreceptors, the cardiopulmonary reflex, the cerebral autoregulation and the CO_2 reactivity regulation. The baroreceptor modeling rules the chronotropic effect, the inotropic effect of both the ventricles, and the

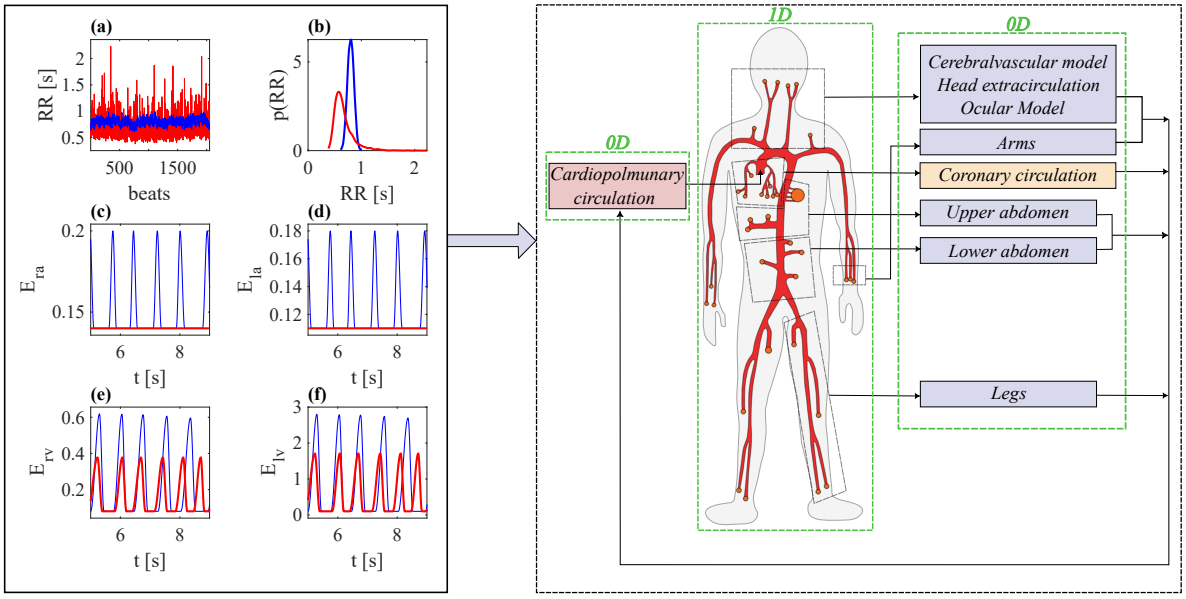

Figure 1: Scheme of the stochastic modeling approach. Left: hemodynamic features of AF (red) versus SR (blue) beating. (a)-(b) RR time-series and probability density functions (pdfs); (c)-(d) right and left atrial elastances, (e)-(f) right and left ventricular elastances (all the elastances are expressed in mmHg/ml). Right: scheme of the 0D-1D cardiovascular model.

regulation of systemic vascular resistances, venous compliances, and venous unstressed volumes. The cardiopulmonary reflex plays the same role as the baroreceptors, except for the inotropic and chronotropic effects. The cerebral autoregulation and CO_2 reactivity regulation control the resistances and compliances of the pial circulation.

A schematic picture of the overall model is shown in the right box of Fig. 1, while details and governing equations are reported in the Supplementary Material.

2.1.1. Ocular Model

The 0D ocular model consists of 6 compartments, each describing a fundamental feature of the ocular circulation. The first compartment is the retrobulbar arachnoid space (rSAS), anatomically located on the posterior eye. While this compartment does not exchange fluids with other compartments, it affects the total ocular volume by employing ICP-driven deformations described by the compliance C_{rg}. The aqueous humor compartment presents an aqueous humor inflow $Q_{aq,in}$, and outflow $Q_{aq,out}$, both connected to the capillary-venous section of the cerebral model. An additional passive compartment accounts for all the eye structures that do not change in volume, such as the lens and vitreous humor. Finally, the eye blood circulation is modeled by employing three compartments connected in series that account for the arterial, capillary, and venous circulation. The circulations of the choroid and retina, which collectively encompass all the eye blood circulation, are lumped together in the three blood compartments.

The equations governing the intraocular pressure (IOP) and the globe volume (V_g) are:

$$\frac{\mathrm{d}IOP}{\mathrm{d}t} = \frac{1}{C_g}\left(C_{rg}\frac{\mathrm{d}ICP}{\mathrm{d}t} + C_{ag}\frac{\mathrm{d}Pa_{eye}}{\mathrm{d}t} + C_{vg}\frac{\mathrm{d}Pv_{eye}}{\mathrm{d}t} + Q_{aq,in} - Q_{aq,out}\right) \tag{1}$$

$$\frac{\mathrm{d}V_g}{\mathrm{d}t} = C_{ag}\frac{\mathrm{d}(Pa_{eye} - IOP)}{\mathrm{d}t} + C_{vg}\frac{\mathrm{d}(Pv_{eye} - IOP)}{\mathrm{d}t} + Q_{aq,in} - Q_{aq,out} \tag{2}$$

The ocular arterial pressure Pa_{eye} is defined as the average pressure between the right and left internal carotids. The ocular venous pressure Pv_{eye} is assimilated to the maximum value between the central venous pressure (CVP) and the episcleral venous pressure (EVP):

$$Pa_{eye} = 0.5\,(P_{ICAl} + P_{ICAr}) - L_{f-b}\rho g \cos\alpha \tag{3}$$

$$EVP = P_{svc} - \rho g \left(\frac{L_H}{2} + \frac{L_{svc}}{2}\right) \sin\alpha - L_{f-b}\rho g \cos\alpha \tag{4}$$

$$Pv_{eye} = \max[CVP, EVP] \tag{5}$$

where $L_{f-b} = 0.03$ m is the perpendicular distance between the globe and the mid-coronal plane; $L_H = 0.15$ m is the vertical anatomical length of the head.

The aqueous humor inflow is set $Q_{aq,in} = 0.048{\cdot}10^{-6}$ l/s, while the aqueous humor outflow rate $Q_{aq,out}$ is defined as:

$$Q_{aq,out} = C_{tm}\,(IOP - EVP) + Q_{uv} \tag{6}$$

where $C_{tm} = 0.0035 \cdot 10^{-6}$ l/(s·mmHg) is the aqueous outflow facility, and Q_{uv} is the uveoscleral outflow. The C_g is the globe compliance, while C_{ag} and C_{vg} are the arterial-globe and venous-globe compliances, respectively, defined as:

$$C_g = V_g \left(\frac{C_1}{IOP} + C_2\right) \tag{7}$$

$$C_{ag} = 0.3V_g \left(\frac{C_1}{IOP} + C_2 - \frac{1}{k_g IOP}\right) \tag{8}$$

$$C_{vg} = 0.7V_g \left(\frac{C_1}{IOP} + C_2 - \frac{1}{k_g IOP}\right) \tag{9}$$

where $C_1 = 4.87 \cdot 10^{-3}$ 1/mmHg, $C_2 = 3.90 \cdot 10^{-5}$ 1/mmHg and $k_g = 312$ [46].

To integrate the ocular model with the global cardiovascular model, arterial eye input (Qa_{eye}) and venous eye output (Qv_{eye}) flow are estimated as:

$$Qa_{eye} = C_{ag} \left(\frac{\mathrm{d}(Pa_{eye} - IOP)}{\mathrm{d}t}\right) + Q_{eye} \tag{10}$$

$$Qv_{eye} = Q_{eye} - C_{vg} \left(\frac{\mathrm{d}(Pv_{eye} - IOP)}{\mathrm{d}t}\right) \tag{11}$$

where Q_{eye} is the eye flow rate and is determined by the equation $Q_{eye} = (Pa_{eye} - Pv_{eye})/R_{eye}$, being R_{eye} the resistance of the capillary bed (represented as a rigid compartment) and set to 4676 mmHg·s/ml. More details on governing equations and parameter setting are offered in the Supplementary Material.

2.2. SR and AF features

The model was employed to inquire into ocular hemodynamics during physiological SR and AF, by simulating the cardiovascular response of a generic healthy young patient in supine posture. To avoid the patient-specific details (e.g., sex, age, weight, and cardiovascular diseases) inherited by real RR beating, we exploited artificially built RR intervals - RR [s] is the cardiac beating period, with the heart rate, $HR = 60/RR$, expressed in [bpm] - in both rhythms, as done in previous studies [29, 31, 33–35].

RR_{SR} intervals in SR configuration were extracted from a correlated pink Gaussian distribution with mean value $\mu_{SR} = 0.857s$ ($HR = 70$ bpm) and a coefficient of variation $cv_{SR} = 0.07$ (see [29, 31, 35, 48] and therein references). The RR_{SR} time-series and the corresponding probability density functions (pdfs) are reported in blue in the left box of Fig. 1, panels (a, b).

Concerning AF, three typical features were included: (i) faster, irregular, and uncorrelated RR beating; (ii) absence of atrial kick; (iii) left and right ventricular systolic dysfunction [31, 32, 35, 36]. The AF beating (RR_{AF}) was obtained by superposing two statistically independent times: the first obtained from a correlated pink Gaussian distribution and the second from an uncorrelated exponential distribution. The RR_{AF} (Figure 1a, red curve) was extracted from the resulting uncorrelated exponentially-modified Gaussian distribution (Figure 1b, red curve), with $\mu_{AF} = 0.67s$ ($HR = 90$ bpm) - as a faster HR is commonly found in AF - $cv_{AF} = 0.26$ [48], and $\gamma = 6$ Hz (see [31, 49, 50] and therein references). The absence of atrial kick, which characterizes the loss of atrial contraction during AF [51, 52], was simulated by imposing a constant left and right atrial elastance (Figure 1, panels c and d, red curves) [31, 32, 35, 36]. In this way, the atria contribution of the ventricles filling (atrial kick) is impaired. Finally, reduced left [53–55] and right [56] ventricular systolic function is generally observed during AF and this aspect was modeled by decreasing both left and right maximum left ventricular elastances by 40 % with respect to their baseline values (Figure 1, panels e and f, red curves). A moderate ventricular impairment was here chosen, given the heterogeneity of clinical [53–56] and modeling [31, 32, 36] literature

in this regard and the difficulty in translating ventricular dysfunction into elastance terms [51].

After the modeling system exceeds the numerical transient (first 50 beats), a total of 2000 beats for each SR and AF condition in supine posture were simulated to guarantee the results reach a statistical stationarity state. For the central hemodynamics validation (see Section 3.1), we considered the following parameters: stroke volume $SV = V_{lved} - V_{lves}$ (where V_{lved} and V_{lves} are left ventricular end-diastolic and end-systolic volumes, respectively), ejection fraction $EF = SV/V_{lved}$, cardiac output $CO = SV \cdot HR$, mean systemic (MAP) and pulmonary (MPAP) arterial pressures. For the ocular hemodynamics (see Section 3.2), we focused on primary ocular variables: the intraocular pressure, IOP, the ocular perfusion pressure, $OPP = Pa_{eye}–IOP$, and the ocular translaminar pressure, $TLP = IOP–ICP$. Such primary variables involve in their definition some auxiliary variables: arterial and venous pressures at the level of the eye, Pa_{eye} and Pv_{eye} (here in supine posture taken as the internal carotid pressure and the central venous pressure, respectively), and intracranial pressure, ICP.

3. Results

To validate our modeling approach, we will first present a comparison on the central hemodynamics between our model findings and available literature regarding SR and AF, see Section 3.1. Then, after an overview of the time-series of ocular variables in SR and AF (Section 3.2.1), we will focus on a beat-to-beat analysis on the ocular hemodynamic alterations induced by AF (Section 3.2.2). The few hemodynamic ocular measures in AF will be discussed in comparison with modeling outcomes in the next sections. We recall that the present model has been recently and extensively validated against posture [43, 46, 47] and gravity [42, 44, 45] changes, as well as in AF conditions [29, 30, 35].

3.1. Model validation with literature data: central hemodynamics

Table 1 compares the present numerical simulations (left columns) with clinical data measured in literature (right columns), in terms of common central hemodynamic parameters. For validation purposes, we choose to show only the parameters that are extensively and reliably measured in the literature. However, it should be recalled that the model can provide many other

	Present simulations						Clinical literature				
	Mean			cv			SR		AF		
	SR	AF	Δ%	SR	AF	$\frac{cv_{\mathrm{AF}}}{cv_{\mathrm{SR}}}$	Mean	Std	Mean	Std	Δ%
HR [bpm]	70	90	28.57	0.07	0.26	3.78	66.84	11.91	81.83	23.44	22.42
SV [ml]	76.31	50.74	-33.51	0.03	0.08	3.23	77.48	25.57	52.13	15.98	-32.72
EF [%]	61.61	42.06	-31.74	0.02	0.07	3.56	63.63	6.90	53.08	12.42	-16.58
CO [l/min]	5.36	4.78	-10.84	0.06	0.21	3.66	5.35	2.28	4.29	1.46	-19.83
MAP [mmHg]	90.74	86.73	-4.42	0.03	0.05	1.92	89.59	12.14	93.90	12.31	4.81
MPAP[mmHg]	15.49	15.48	-0.12	0.02	0.05	2.47	19.06	8.51	21.51	7.25	12.87

Table 1: Central hemodynamics: present numerical simulations (left) against clinical literature (right). Heart rate (HR), stroke volume (SV), ejection fraction (EF), cardiac output (CO), mean arterial pressure (MAP), and mean pulmonary arterial pressure ($MPAP$) are listed. The simulations column reports the mean and the coefficient of variation (cv) of each signal, along with the percentage differences between the SR and AF mean values and the cv ratios in AF and SR conditions. Statistically significant differences were found between SR and AF values for all signals by means of the Wilcoxon test ($p<0.01$). The clinical literature column provides the mean and standard deviation (Std) of the available data in literature, and the percentage differences between the SR and AF mean values.

cardiovascular details (such as cardiac-coronary hemodynamics, cerebral circulation, arterial patterns and venous return), here not displayed because out of the validation scope. The mean and coefficient of variation (cv) values obtained with the model are computed over 2000 beats in SR and AF (cv is the ratio between standard deviation and mean values). For literature data reported in Table 1, the mean value is computed as the average value among the cited studies and weighted over the sample size of each, while standard deviation (Std) is computed as referred to the weighted mean value. Table SM11 in the Supplementary Material reports detailed values and references for each literature study here exploited for validation. In order to better display the range of variability of the clinical data, Fig. 2 shows the variations from SR to AF of the parameters measured in the literature (Mean±Std) and simulated (mean) by the model, as reported in Table 1.

Although HR is an input parameter imposed in our analysis (and not directly exploitable for validation), a first preliminary comment is due. Literature results show an overall mean increase in HR around +22%, when passing from SR to AF. Thus, the here modelled HR mean increase from 70 to 90 bpm (about +29%) when passing from SR to AF realistically mimics the well-known feature of accelerated beating, which is generally found in AF and documented in literature.

Figure 2 makes evident that, for both SR and AF configurations and all the parameters analyzed, the mean values predicted by the model (red crosses) fall within the measurement range [Mean - Std, Mean + Std] given by the clinical literature (black lines). More in details, in clinical literature both stroke volume, SV, and ejection fraction, EF, exhibit a remarkable decrease (-33% and -17%, respectively). In good agreement with measurements, our model predicts a relevant decrease in AF: -34% and -32% for SV and EF, respectively. SV (and consequently EF) reduction is due to three main mechanisms all implemented in our model to simulate AF: (i) HR increase, which reduces the necessary time to adequate ventricular emptying and filling; (ii) absence of atrial kick, responsible of the ventricular filling for about 20%; and (iii) reduced ventricular contractility (i.e., ventricular systolic dysfunction). The fact that EF decreases more in the model (-32%) than in literature (-17%) is due to the interplay between increased HR (which decreases V_{lved}) and ventricular systolic dysfunction (which increases V_{lved} [36]), resulting in a slight change of V_{lved} in AF, thus inducing a marked EF reduction in AF. Cardiac output, CO, is measured to reduce by about 20% on average during AF, in front of a mean reduction in AF of about 11% predicted by the modeling approach. A smaller reduction in CO (-11%) compared to the literature (-20%), can be due to a greater increase of HR during AF in our model (+29%) compared to the measurements in the literature (+22%). In fact, given a similar SV reduction (-34% model, -33% clinical literature), a higher HR mitigates the CO reduction.

Mean systemic (MAP) and pulmonary ($MPAP$) arterial pressure values per beat are perhaps the most controversial hemodynamics variables in AF, since the heart rate variability causes problems to oscillometric instruments and noninvasive blood pressure measurements [31]. MAP slightly increases during measured AF (+5%), while the model predicts a quite negligible reduction (-4%). As for $MPAP$, the mean value is observed to mildly increase in AF measurements (+13%), while no variation emerges from our numerical results. The overall picture is that the marginal variations for MAP and $MPAP$ observed by the model are due to the action of baroreceptors and cardiopulmonary receptors, which maintain in AF the levels of central mean pressures close to the physiological values of the SR. These modest variations highlighted by the model fall within the range of variability of the data measured in the literature, as shown in Fig. 2.

In addition to the mean values of the hemodynamic parameters evaluated over 2000 simulated beats and compared with the literature, Table 1 also

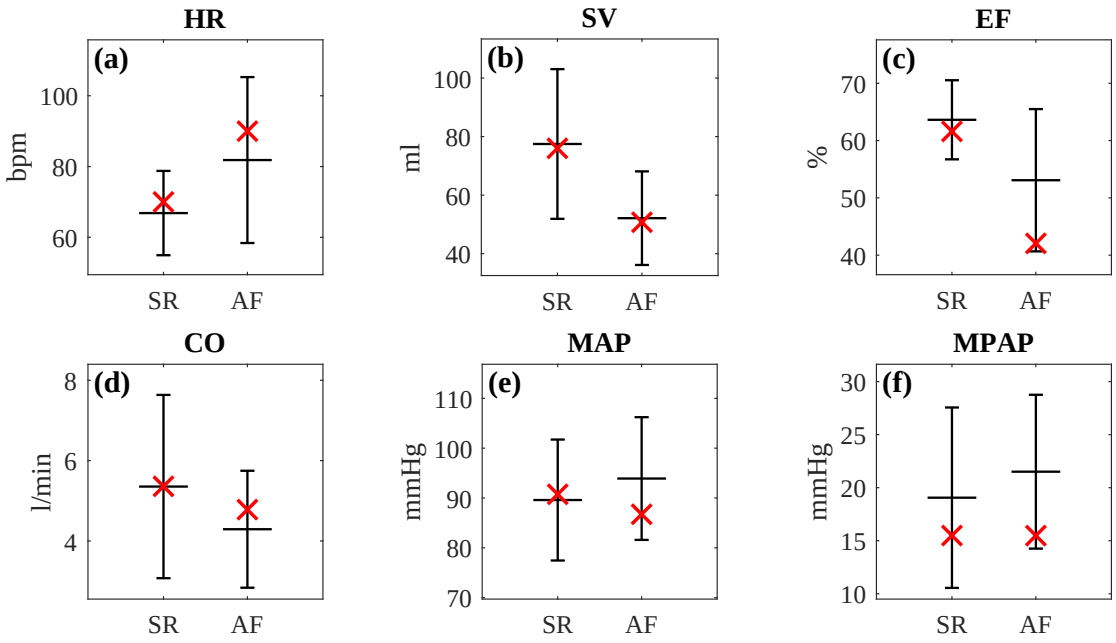

Figure 2: Central hemodynamics in SR and AF: present numerical simulations (red crosses) against the range of variability [Mean - Std, Mean + Std] given by the clinical literature (black lines). (a) Heart rate, HR; (b) stroke volume, SV; (c) ejection fraction, EF; (d) cardiac output, CO; (e) mean systemic arterial pressure, MAP; (f) mean pulmonary arterial pressure, MPAP.

reports the cv values obtained from these simulations. All the parameters show a more marked variability in AF than SR. It can be observed that the higher RR variability imposed (cv=0.07 in SR, cv=0.26 in AF) result in cv values in AF about 1.9-3.8 times higher than SR. The lowest cv_{AF}/cv_{SR} ratios are found for MAP (1.9) and $MPAP$ (2.5), again confirming the ability of short-term autoregulation mechanisms to counteract AF-induced alterations at central (systemic and pulmonary) pressures level.

3.2. Ocular hemodynamics in SR and AF

3.2.1. Overview of the ocular variables

To introduce the ocular hemodynamic response to AF, Fig. 3 shows representative time-series of primary (IOP, OPP, TLP) and auxiliary (Pa_{eye}, Pv_{eye}, ICP) variables, as simulated in SR and AF. We will first explain the behavior of the primary variables as a function of the auxiliary ones, and then we will compare the trends in AF (red curves) with those in SR (blue curves).

As displayed in Eq. (1), IOP in supine posture depends on Pa_{eye}, Pv_{eye}, and ICP. Since the retrobulbar subarachnoid space-to-globe compliance, C_{rg}, is two orders of magnitude lower than the arterial, C_{ag}, and venous, C_{vg}, blood-to-globe compliances, time derivatives of Pa_{eye} and Pv_{eye} terms basically rule the IOP dynamics. Between these two differential terms, given the much higher arterial wave amplitude with respect to the venous one (see panels a and b of Fig. 3), IOP is mainly governed by Pa_{eye}. The significant dependence of IOP on Pa_{eye} was already observed considering posture changes [46]. To this end, a law linking IOP variations only to changes of blood pressure at the level of the eye has been proposed, which is consistent with the understanding that acute IOP changes result from gravitationally driven blood pressure changes [57]. The strong $IOP(Pa_{eye})$ link is here confirmed also in supine condition, as can be observed comparing panels (a) and (e) of Fig. 3, and considering that the Pearson correlation coefficient between Pa_{eye} and IOP time-series is 0.99 in both SR and AF.

As IOP time-series is strongly correlated to Pa_{eye}, OPP due to its definition ($Pa_{eye} - IOP$) is in turn strictly linked to Pa_{eye}. Panels (a), (e), and (c) clearly show very similar trends for Pa_{eye}, IOP, and OPP times-series, respectively. We recall that OPP, being a pressure difference, is a measure of the ocular perfusion and its decrease has been associated to an augmented risk for glaucoma according to the vascular theory [7].

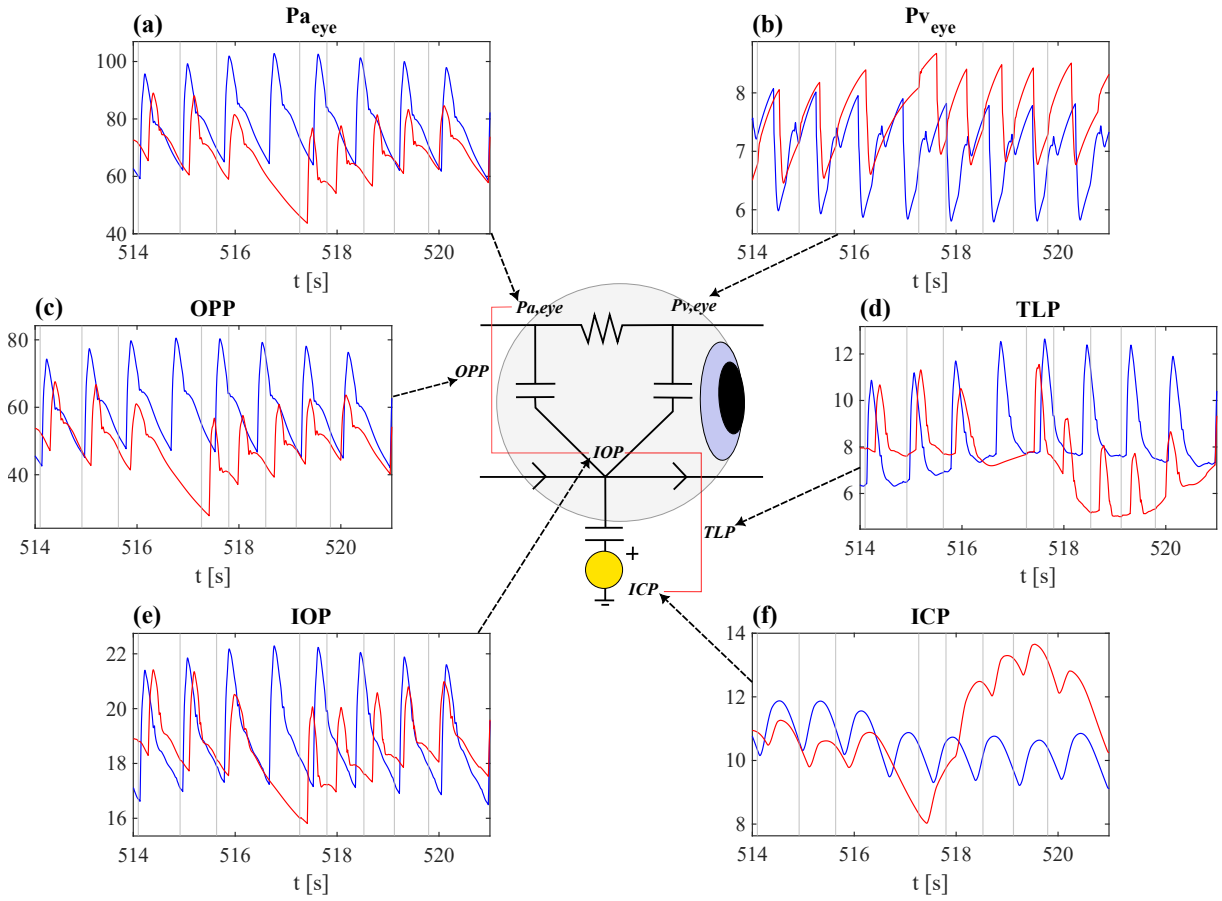

Figure 3: Representative time-series of primary and auxiliary ocular variables in SR (blue curves) and AF (red curves): (a) Pa_{eye}, (b) Pv_{eye}, (c) OPP, (d) TLP, (e) IOP, (f) ICP. All variables are expressed in mmHg.

In the end, the ocular translaminar pressure TLP is driven mainly by IOP - especially regarding the pulsatile waveform pattern in SR (please, compare blue curves in panels (e) and (d) of Fig. 3) - as confirmed by the Pearson correlation coefficient between TLP and IOP, that results ρ=0.93 in SR, ρ=0.81 in AF. However, ICP has a non-negligible effect on TLP (Pearson correlation coefficient between TLP and ICP, ρ=-0.34 in SR, ρ=-0.49 in AF), which is more evident in the increasing/decreasing wave patterns over several beats occurring in AF (please, compare red curves in panels (d) and (f) of Fig. 3). Notice that TLP is a marker for increased glaucoma risk, being TLP higher in glaucoma patients [8, 9].

Comparing AF with respect to SR, all signals exhibit a higher variability in AF, by reaching lower diastolic values (and greater wave amplitude) after long beats and higher systolic values (and smaller wave amplitude) after short beats. This is especially true for cardiac (Pv_{eye}) and proximal (Pa_{eye}) signals, as well as signals ruled by central hemodynamics, that is IOP and OPP. For these four signals (panels (a), (b), (c), (e)), the alteration induced by one (short or long) beat is almost completely absorbed within the subsequent 1-2 beats. Differently, in the case of TLP, where the influence of the distal ICP signal is not negligible, the AF-induced variability is not recovered on a single beat scale, but gives rise to ascending/descending patterns over several beats (see panels (d) and (f)). This behavior is entirely attributable to the distal cerebral hemodynamics, on which ICP strongly depends. Due to the complex temporal interplay of distal resistances and compliances acting like springs in series and parallel, it has been observed that during AF in the cerebral microcirculation the latency in recovering the equilibrium state is much higher than at proximal level [24, 26]. As a consequence, when the AF irregularity propagates towards the distal regions, ICP and related variables remain altered for longer, as clearly visible in panels (d) and (f) of Fig. 3.

3.2.2. Beat-to-beat analysis: mean and pulse values

To quantify the AF-induced variability qualitatively described in the previous section, we here propose a beat-to-beat analysis on the primary and auxiliary ocular variables in which we investigate the mean and pulsatile (defined as maximum minus minimum) values calculated over the beat.

Table 2 reports mean and cv values of beat-averaged ocular variables, together with percentage variations of mean values and cv ratios between AF and SR. Mean values of all primary and auxiliary variables show modest (within 8%) variations between SR and AF, while cv ratios between AF and

	Mean			cv		
	SR	AF	Δ%	SR	AF	$\frac{cv_{\mathrm{AF}}}{cv_{\mathrm{SR}}}$
$\mathrm{Pa_{eye}}$[mmHg]	77.16	72.94	-5.47	0.03	0.06	1.91
$\mathrm{Pv_{eye}}$[mmHg]	6.99	7.38	5.52	0.01	0.03	2.23
ICP[mmHg]	10.50	10.88	3.60	0.03	0.07	2.32
IOP[mmHg]	18.81	19.20	2.04	0.02	0.03	1.71
OPP[mmHg]	58.34	53.74	-7.89	0.03	0.07	1.97
TLP[mmHg]	8.31	8.32	0.07	0.05	0.09	2.00

Table 2: Mean and coefficient of variation (cv) values of beat-averaged ocular variables in SR and AF conditions. Percentage variations between the mean values in SR and AF conditions and ratios between cv values in AF and SR are reported. All variables show a statistical significant difference (Wilcoxon test) between SR and AF with p-value<0.01, with the only exception of TLP (p-value=0.025).

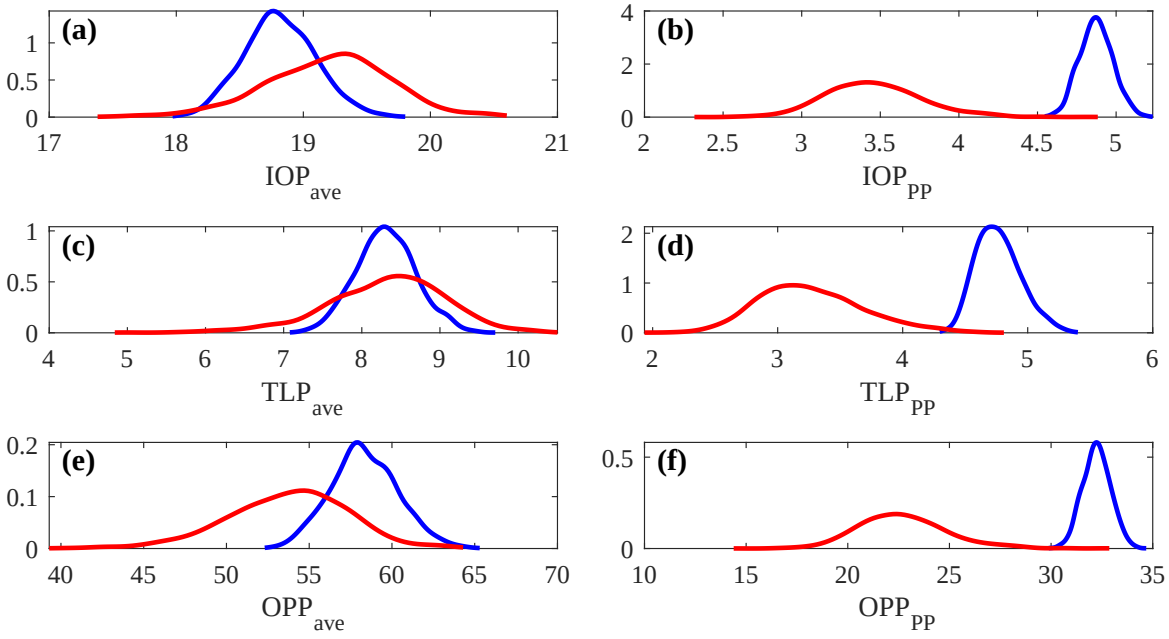

Figure 4: Probability density functions of beat-averaged (left panels) and pulse (right panels) values of primary ocular variables (IOP, TLP, OPP), in SR (blue curves) and AF (red curves). All variables are expressed in mmHg.

	Mean			cv		
	SR	AF	$\Delta\%$	SR	AF	$\frac{cv_{\mathrm{AF}}}{cv_{\mathrm{SR}}}$
$\mathrm{Pa_{eye}}$[mmHg]	37.12	26.16	-29.53	0.02	0.10	4.50
$\mathrm{Pv_{eye}}$[mmHg]	2.02	1.59	-21.23	0.03	0.08	3.27
ICP[mmHg]	1.51	0.84	-44.29	0.12	0.32	2.72
IOP[mmHg]	4.87	3.46	-29.00	0.02	0.09	4.14
OPP[mmHg]	32.24	22.70	-29.60	0.02	0.10	4.55
TLP[mmHg]	4.77	3.27	-31.48	0.04	0.13	3.40

Table 3: Mean and coefficient of variation (cv) values for the pulsatile pressures of the ocular variables in SR and AF conditions. Percentage variations between the mean values in SR and AF conditions and ratios between cv values in AF and SR are reported. All variables show a statistical significant difference (Wilcoxon test) between SR and AF with p-value<0.01.

SR vary from 1.7 to 2.3. The slight mean variation and the much more marked variability of beat-averaged values in AF is also observable in the probability density functions of Fig. 4, where in the left panels distributions of beat-averaged values of primary ocular variables (IOP, TLP, OPP) are displayed in SR (blue) and AF (red) conditions. In fact, although SR and AF distributions are centered around comparable mean values (the highest variation around 8% is found for OPP, which reduces as a combination of Pa_{eye} decrease and IOP increase), the probability of reaching very high/low beat-averaged values substantially increases in AF.

Table 3 shows mean and cv values of pulsatile pressure for ocular variables, as well as percentage variations and ratios between AF and SR. Pulsatile pressure mean values overall decrease in AF for all the variables observed and this is mainly induced by the reduction of SV (about - 33%) and central aortic pulse pressure (about -31%). More in details, primary ocular variables (and also Pa_{eye}, which is an important determinant of them) experience mean pulse pressure reduction around 30%, which is close to those observed by SV and central aortic pulse pressure. Pv_{eye} shows smaller mean pulse pressure variations in AF (about -21%), probably due to the nature of retrograde pulsatility characterizing venous signals more similarly in SR and AF. ICP is instead the variable with the greatest pulsatility reduction in AF (over -44%) as a consequence of the same mechanism - explained in

the previous section - of the greater latency of the cerebral microcirculation in recovering the equilibrium state, which therefore further amplifies the signal alteration (i.e., pulse pressure reduction) compared to what happens in the proximal region (Pa_{eye}) [24, 26]. We recall that pulsatile pressure yields important information, and it is difficult to be *in vivo* monitored for such cerebro-ocular variables. Indeed, current techniques assessing the ocular blood flow - such as laser Doppler flowmeter and optical coherence tomography angiography - present limited temporal resolution which allows only mean blood flow to be computed. Laser speckle contrast imaging - providing diastole-to-systole perfusion - is a promising technique, however the management of filtering movement artifacts and the choice of exposure time make it still not entirely suitable for large-scale use. Thus, clinical literature typically reports only beat-averaged values. The overall mean pulsatile pressure reduction in AF is itself an index of reduced variability, as the hemodynamic signals damp their maximum-to-minimum range. This outcome is enriched by the cv value of pulsatile pressures per beat. The ratio cv_{AF}/cv_{SR}, spreading between 2.7 and 4.5, evidences a high pulsatile pressure variability in AF. This means that the probability of having very high or low pulsatile values markedly increases in AF with respect to SR.

Right panels of Fig. 4 display probability density functions of pulsatile values for primary ocular variables (IOP, TLP, OPP) in SR (blue) and AF (red) conditions. By graphically highlighting the statistics of Table 3, the distributions show that in AF the probability of having spread and reduced pulsatile values significantly increases for the three variables, so that reaching physiological values of pulsatile pressures in AF is extremely rare (right tails in AF barely reach SR mean values).

4. Discussion

Let us focus on the two ocular parameters OPP and TLP, by means of beat-averaged and pulsatile values. Our simulations show that mean values of beat-averaged OPP and TLP slightly differ in AF and SR, while cv values markedly increase in AF. This implies that mean perfusion and tensive level are maintained in AF at an adequate level similar to SR. However, the increased variability in AF results in a higher probability of possible transient hypoperfusions (low OPP) and hypertensive events (high TLP), which are potential sources of ocular stress. Although some studies observed that high

pulsatile variability could be detrimental at ocular level [58–61], literature is still debated so that no clear clinical implications can be drawn.

Pulsatile values decrease on average by about 30% for both OPP and TLP in AF, thus signals amplitude is damped with respect to SR. The main driver of this mechanism is the reduced central pressure pulsatility, which in turn is induced by the SV reduction (recall that SV is proportional to the central pulsatile pressure [62]). The pulsatility damping at ocular level is found with the same magnitude as present at central level (the pulsatility of both OPP and TLP reduces around -30% similarly to SV), and alteration or dysfunction of short-term regulatory mechanisms (such as dysautonomia) can further enhance these changes. The reduction of mean pulsatile values for OPP and TLP, being itself a marker of reduced variability, should be accounted for together with the strong increase of cv values by 3.5 to 4.5 times in AF. The combination of these two mechanisms (mean value decrease and cv value increase of beat pulsatility) decreases the probability of having physiological pulsatile OPP and TLP values in AF, as evidenced by the pdfs in right panels of Fig. 4. Pulsatile pressure - which can be easily deduced by the modeling approach but hardly measured *in vivo* - is a crucial parameter to enrich the description of the hemodynamic variability induced by AF. Although there is no clear threshold level of pulsatility reduction beyond which ocular damage can occur, we recall that myocardial contractility reduction is considered clinically relevant when EF drops 20% or more [62]. Thus, we can assume that ocular pulsatility reduction of 20% or more, as happens for OPP and TLP, can be as well clinically relevant.

To further understand the link between ocular hemodynamics and heartbeating - which is a fundamental aspect in AF as RR beats are accelerated, uncorrelated and much more disperse – Fig. 5 shows scatteplots of beat-averaged (left panels) and pulsatile (right panels) values of TLP and OPP as function of the previous RRs (i.e., the RR value of the current beat and the TLP and OPP value of the next beat are the coordinates of each point in the scatterplots). It can be noted that: (i) beat-averaged and pulsatile values for both TLP and OPP are quite sparse in SR, as the coefficient of variation, R^2, does not exceed 0.3; (ii) for pulsatile values (right panels) the correlation with the previous RR increases in AF, as R^2 is beyond 0.5 for both OPP and TLP.

By combining the analysis beat-averaged and pulsatile values (Tables 2 and 3, respectively, and Figure 4) together with scatterplots, the overall picture emerging in AF with respect to SR for TLP and OPP is the following:

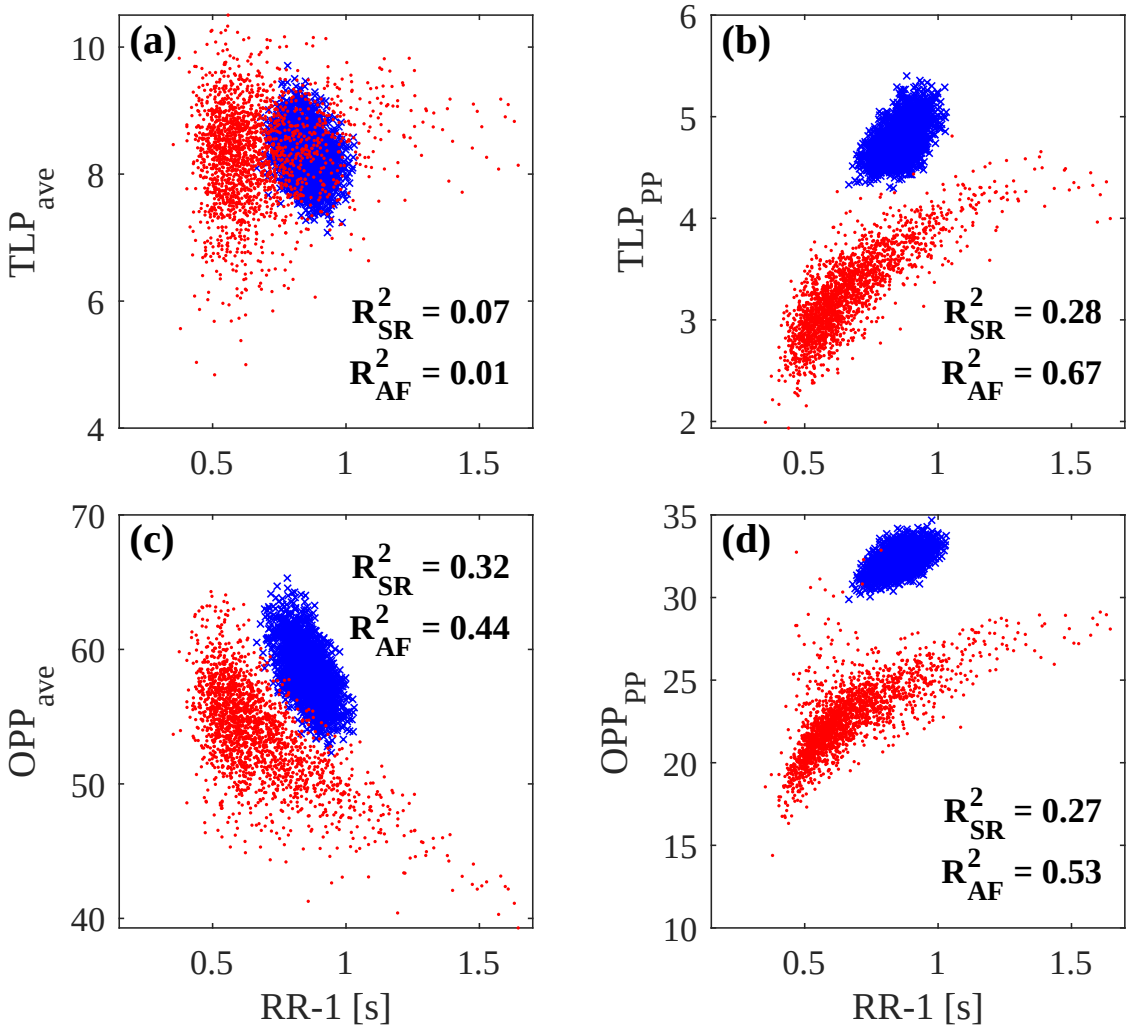

Figure 5: Scatterplots of beat-averaged values and RR (left panels), pulsatile values and RR (right panels), with the corresponding coefficients of determination, R^2, in SR (blue curves) and AF (red curves). Top panels: TLP. Bottom panels: OPP.

- TLP. Beat-averaged values show no correlation with RR (R^2=0.01) and their mean value remains constant, even if the distribution is more spread enhancing the probability of very high or low values. Instead, mean pulsatile value decreases significantly. In particular, given the positive correlation (R^2=0.67) between pulsatile values and RR, short beats (which are the majority in the distribution) give rise to an adequate beat-averaged value (see panel 5a), though are not able to temporarily guarantee a physiological perfusion due to the extremely reduced pulsatility (see panel 5b). On the other hand, only very long beats (although AF-induced and out-of-range with respect to SR) provide a nearly physiological TLP response for both beat-averaged and pulsatile values.

- OPP. Beat-averaged values evidence a negative correlation with RR (R^2=0.44) and their mean value slightly decreases. Mean pulsatile values markedly decrease and (similarly to TLP) pusatile values are correlated with RR (R^2=0.53). This framework induces possible transient ocular hypoperfusions and hypo-pulsatility events triggered by two mechanisms (see panels (see panel 5c-d)): (i) for long beats, pulsatile value is almost in the physiological range, but beat-averaged perfusion is lower than normal; (ii) for short beats, beat-averaged level is adequate, but pulsatility is too damped to guarantee a physiological excursion range.

In short, from a hypoperfusion viewpoint, short beats are the most hazardous for TLP, while both short and long beats are risky for OPP. We recall that, according to the vascular theory [7], an OPP decrease has been associated to an augmented risk for glaucoma. However, clinical literature investigating the link between OPP and glaucoma is debated, as in subjects with glaucoma OPP is found to increase [10–12], remain equal [13–15], and reduce [16–18], with respect to the control population. Thus, definitive findings either confirming or refuting the vascular theory are not available to date.

In vivo measurements investigating the role of AF on the ocular hemodynamics are very few and for these reaching a clear overall picture is even more difficult. Some studies concluded that a significant association between AF and glaucoma development exists [19, 20], even if results on IOP are contrasting, showing a modest increase [21], but also a reduction [22]. In this

clinical picture, the present model reveals a very modest mean IOP increase which, combined to a more consistent Pa_{eye} reduction, leads to an average OPP decrease by 8%. However, our model unveils that reduced ocular perfusion can also be achieved by a waveform damping mechanism related to the reduction of the signal pulsatility, which to the best of our knowledge is not reported in literature as hardly measurable. The OPP amplitude decrease captured by the model can yield, especially for short beats, hypo-pulsatility events due to the non-physiological excursion range. If the overall emerging picture is interpreted in view of the vascular theory, present modeling findings suggest that AF-induced hemodynamic changes can increase the risk of glaucoma development. Finally, the marked pulsatility variability (i.e., the alternation of hypo/hyper-tensive or hypo/hyer-perfusive events on the single-beat scale), although not clinically investigated due to experimental difficulties, could *per se* abnormally stimulate the ocular hemodynamics. If the link between AF and glaucoma is confirmed, detection of optimal (rate or rhythm control) strategies in AF management - with their subsequent early adoption - can in turn reduce AF-related risk of glaucoma or minimize ocular hemodynamic changes, with an important impact on the burden of health care costs and quality of life.

The present work has some limiting aspects. First, we focused on the most frequent and typical AF configuration, chosen as representative after a detailed literature review of the most common AF features. More specific cases - such as, for example, bimodal RR probability distributions or much higher ventricular rates - were not accounted here. As we are interested in the net and specific role of AF on the ocular hemodynamics which - without a computational approach - would be hardly identifiable, we accounted for a generic healthy subject experiencing an episode of paroxysmal AF and we evaluated the acute hemodynamic response. Long-term hemodynamic remodeling effects (e.g., atrial enlargement) and concomitant pathologies - such as hypertension, diabetes, mitral stenosis/regurgitation - which usually accompany chronic AF were not considered here and can be included in future works, together with subject-specific features and higher ventricular rates.

5. Conclusions

Through a validated cardiovascular multiscale modeling approach, we observed that during AF ocular perfusion and pressure remain on average quite

adequate, guaranteeing physiological mean values with respect to SR. However, transient relevant hypoperfusions (for OPP) and hypertensive events (for TLP) can occur, due to the high cv value of beat-averaged variables. According to the vascular theory, decreased OPP and increased TLP are potential markers associated to the increased risk of glaucoma development. Moreover, ocular hemodynamic signals modify their waveforms in AF, by significantly reducing their amplitude. This, in addition to the high variability of pulsatile pressure, may lead to episodes of OPP transient hypo-pulsatility due to the inadequate signal amplitude. Awaiting necessary clinical data which are to date lacking, the present study can boost clinical measurement of specific and more targeted parameters (e.g., ocular pulsatility indexes) and at the same time enrich - through mechanistic and hemodynamic-driven hints in the AF framework - the vascular theory relating reduced ocular perfusion and increased risk of glaucoma. In this context, present findings suggest that AF may play a role in augmenting the development of glaucoma.

Declaration of competing interest

The authors declare that they have no known competing financial interests or personal relationships that could have appeared to influence the work reported in this paper.

Acknowledgments

This study was carried out within the 2022EAN2BB "Cerebral fluid dynamics: investigating the association between atrial fibrillation and dementia through an integrated in silico-in vivo framework" project – funded by the Ministero dell'Università e della Ricerca – within the PRIN 2022 program (D.D.104 - 02/02/2022). This manuscript reflects only the authors' views and opinions and the Ministry cannot be considered responsible for them.

References

[1] G. A. Roth, G. A. Mensah, C. O. Johnson, G. Addolorato, E. Ammirati, L. M. Baddour *et al.*, Global burden of cardiovascular diseases and risk factors, 1990-2019: Update from the gbd 2019 study, J. Am. Coll. Cardiol. 76(25) (2020) 2982–3021.

[2] G. Hindricks, T. Potpara, N. Dagres, E. Arbelo, J. J. Bax, C. Blomström-Lundqvist *et al.*, 2020 ESC guidelines for the diagnosis and management of atrial fibrillation developed in collaboration with the european association for cardio-thoracic surgery (EACTS), Eur. Heart J. 42(5) (2021) 373–498.

[3] L. Rivard, L. Friberg, D. Conen, J. S. Healey, T. Berge, G. Boriani *et al.*, Atrial fibrillation and dementia: A report from the AF-SCREEN international collaboration, Circulation 145(5) (2022) 392–409.

[4] V. Jacobs, M. J. Cutler, J. D. Day, T. J. Bunch, Atrial fibrillation and dementia, Trends Cardiovasc. Med. 25(1) (2014) 44–51.

[5] A. Kanmanthareddy, A. Vallakati, A. Sridhar, M. Reddy, H. P. Sanjani, J. Pillarisetti *et al.*, The impact of atrial fibrillation and its treatment on dementia, Curr. Cardiol. Rep. 16 (2014) 519.

[6] F. Da Silva, M. Lira, Intraocular pressure measurement: A review, Surv. Ophthalmol. 67(5) (2022) 1319–1331.

[7] J. Flammer, S. Orgül, V. Costa, N. Orzalesi, G. K. Krieglstein, L. M. Serra *et al.*, The impact of ocular blood flow in glaucoma, Prog. Retin. Eye Res. 21(4) (2002) 359–393.

[8] L. Siaudvytyte, I. Januleviciene, A. Daveckaite, A. Ragauskas, L. Bartusis, J. Kucinoviene *et al.*, Literature review and meta-analysis of translaminar pressure difference in open-angle glaucoma, Eye 29(10) (2015) 1242–1250.

[9] L. Siaudvytyte, I. Januleviciene, A. Ragauskas, L. Bartusis, I. Meiliuniene, B. Siesky *et al.*, The difference in translaminar pressure gradient and neuroretinal rim area in glaucoma and healthy subjects, J. Ophthalmol. 2014 (2014) 937360.

[10] L. Abegão Pinto, K. Willekens, K. Van Keer, A. Shibesh, G. Molenberghs, E. Vandewalle *et al.*, Ocular blood flow in glaucoma – the leuven eye study, Acta Ophthalmol. 94(6) (2016) 592—-598.

[11] L. Abegão Pinto, E. Vandewalle, K. Willekens, C. Marques-Neves, I. Stalmans, Ocular pulse amplitude and doppler waveform analysis in glaucoma patients, Acta Ophthalmol. 92(4) (2014) e280–e285.

[12] K. Willekens, L. Abegão Pinto, E. Vandewalle, C. Marques-Neves, I. Stalmans, Higher optic nerve sheath diameters are associated with lower ocular blood flow velocities in glaucoma patients, Graef. Arch. Clin. Exp. Ophthalmol. 252(3) (477–483) 2014.

[13] M. Hidalgo-Aguirre, S. Costantino, M. Lesk, Pilot study of the pulsatile neuro-peripapillary retinal deformation in glaucoma and its relationship with glaucoma risk factors, Curr. Eye Res. 42(12) (2017) 1620–1627.

[14] I. Goharian, S. M. Iverson, R. C. Ruiz, K. Kishor, D. S. Greenfield, M. Sehi, Reproducibility of retinal oxygen saturation in normal and treated glaucomatous eyes, Brit. J. Ophthalmol. 99(3) (2015) 318–322.

[15] P. Krzyzanowska-Berkowska, K. Czajor, D. R. Iskander, Associating the biomarkers of ocular blood flow with lamina cribrosa parameters in normotensive glaucoma suspects. comparison to glaucoma patients and healthy controls, Plos One 16(3) (2021) e0248851.

[16] Y. Gao, B. Wan, P. Li, Y. Zhang, X. Tang, Short-term reproducibility of intraocular pressure and ocular perfusion pressure measurements in chinese volunteers and glaucoma patients, BMC Ophthalmol. 16(1) (2016) 145.

[17] A. Samsudin, N. Isaacs, M.-L. S. Tai, N. Ramli, Z. Mimiwati, M. M. Choo, Ocular perfusion pressure and ophthalmic artery flow in patients with normal tension glaucoma, BMC Ophthalmol. 16(1) (2016) 39.

[18] M. Modrzejewska, W. Grzesiak, D. Zaborski, A. Modrzejewska, The role of lipid dysregulation and vascular risk factors in glaucomatous retrobulbar circulation, Bosnian J. Basic Med. 15(2) (2015) 50–56.

[19] H.-K. Cho, J. Han, J. Choi, J. Chae, R. Kim, Association between atrial fibrillation and the risk of glaucoma development: a 12-year nationwide cohort study, Eye 37(10) (2023) 2033–2041.

[20] Y. Suzuki, M. Kiyosawa, Cardiac hypertrophy may be a risk factor for the development and severity of glaucoma, Biomedicines 10(3) (2022) 677.

[21] A. Zaleska-Żmijewska, M. Janiszewski, Z. M. Wawrzyniak, M. Kuch, J. Szaflik, J. P. Szaflik, Is atrial fibrillation a risk factor for normal-tension glaucoma?, Medicine 96(43) (2017) e8347.

[22] R. Peräsalo, C. Raitta, J. Peräsalo, Optic nerve fiber loss in relation to atrial fibrillation and blood pressure, Int. Ophthalmol. 16(4-5) (1992) 259–263.

[23] T. J. Hunter, J. J. Joseph, U. Anazodo, S. R. Kharche, C. W. McIntyre, D. Goldman, Atrial fibrillation and anterior cerebral artery absence reduce cerebral perfusion: A de novo hemodynamic model, Applied Sciences 12(3) (2022) 1750.

[24] M. Anselmino, S. Scarsoglio, A. Saglietto, F. Gaita, L. Ridolfi, Transient cerebral hypoperfusion and hypertensive events during atrial fibrillation: A plausible mechanism for cognitive impairment, Sci. Rep. 6(1) (2016) 28635.

[25] A. Saglietto, S. Scarsoglio, L. Ridolfi, F. Gaita, M. Anselmino, Higher ventricular rate during atrial fibrillation relates to increased cerebral hypoperfusions and hypertensive events, Sci. Rep. 9(1) (2019) 3779.

[26] S. Scarsoglio, A. Saglietto, M. Anselmino, F. Gaita, L. Ridolfi, Alteration of cerebrovascular haemodynamic patterns due to atrial fibrillation: An in silico investigation, J. R. Soc. Interface 14(129) (2017) 20170180.

[27] S. Scarsoglio, A. Saglietto, F. Tripoli, J. J. M. Zwanenburg, G. J. Biessels, G. M. De Ferrari, *et al.*, Cerebral hemodynamics during atrial fibrillation: computational fluid dynamics analysis of lenticulostriate arteries using 7 T high-resolution magnetic resonance imaging, Phys. Fluids 34(12) (2022) 121909.

[28] A. Saglietto, F. Tripoli, J. J. M. Zwanenburg, G. J. Biessels, G. M. De Ferrari, M. Anselmino, *et al.*, Role of the vessel morphology on the lenticulostriate arteries hemodynamics during atrial fibrillation: A CFD-based multivariate regression analysis, Comput. Meth. Prog. Bio. 254 (2024) 108303.

[29] A. Saglietto, M. Fois, L. Ridolfi, G. M. De Ferrari, M. Anselmino, S. Scarsoglio, A computational analysis of atrial fibrillation effects on

coronary perfusion across the different myocardial layers, Sci. Rep. 12(1) (2022) 841.

[30] S. Scarsoglio, C. Gallo, A. Saglietto, L. Ridolfi, M. Anselmino, Impaired coronary blood flow at higher heart rates during atrial fibrillation: investigation via multiscale modelling, Comput. Meth. Prog. Bio. 175 (2019) 95–102.

[31] S. Scarsoglio, A. Guala, C. Camporeale, L. Ridolfi, Impact of atrial fibrillation on the cardiovascular system through a lumped-parameter approach, Med. Biol. Eng. Comput. 52(11) (2014) 905–920.

[32] M. Corti, A. Zingaro, L. Dede, A. M. Quarteroni, Impact of atrial fibrillation on left atrium haemodynamics: A computational fluid dynamics study, Comput. Biol. Med. 150 (2022) 106143.

[33] S. Scarsoglio, C. Camporeale, A. Guala, L. Ridolfi, Fluid dynamics of heart valves during atrial fibrillation: a lumped parameter-based approach, Comput. Methods Biomech. Biomed. Engin. 10(19) (2016) 1060–1068.

[34] S. Scarsoglio, A. Saglietto, F. Gaita, L. Ridolfi, M. Anselmino, Computational fluid dynamics modelling of left valvular heart diseases during atrial fibrillation, PeerJ 4 (2016) e2240.

[35] S. Scarsoglio, C. Gallo, L. Ridolfi, Effects of atrial fibrillation on the arterial fluid dynamics: A modelling perspective, Meccanica 53 (13) (2018) 3251–3267.

[36] A. Deyranlou, J. H. Naish, C. A. Miller, A. Revell, A. Keshmiri, Numerical study of atrial fibrillation effects on flow distribution in aortic circulation, Ann. Biomed. Eng. 48(4) (2020) 1291–1308.

[37] A. Deyranlou, C. A. Miller, A. Revell, A. Keshmiri, Effects of ageing on aortic circulation during atrial fibrillation; a numerical study on different aortic morphologies, Ann. Biomed. Eng. 49(9) (2021) 2196–2213.

[38] L. Zhang, M. Gay, Characterizing left atrial appendage functions in sinus rhythm and atrial fibrillation using computational models, J. Biomech. 41(11) (2008) 2515–2523.

[39] A. Masci, L. Barone, L. Dedè, M. Fedele, C. Tomasi, A. Quarteroni, *et al.*, The impact of left atrium appendage morphology on stroke risk assessment in atrial fibrillation: A computational fluid dynamics study, Front. Physiol. 9 (2019) 1938.

[40] G. Musotto, A. Monteleone, D. Vella, B. Zuccarello, R. Cannova, A. Cook, *et al.*, Fluid-structure interaction analysis of the thromboembolic risk in the left atrial appendage under atrial fibrillation: Effect of hemodynamics and morphological features, Comput. Meth. Prog. Bio. 246 (2024) 108056.

[41] C. Gallo, J. Olbers, L. Ridolfi, S. Scarsoglio, N. Witt, Testing a patient-specific in-silico model to noninvasively estimate central blood pressure, Cardiovasc. Eng. Techn. 12(2) (2021) 144–157.

[42] C. Gallo, L. Ridolfi, S. Scarsoglio, Cardiovascular deconditioning during long-term spaceflight through multiscale modeling, npj Microgravity 6(1) (2020) 27.

[43] M. Fois, S. V. Maule, M. Giudici, M. Valente, L. Ridolfi, S. Scarsoglio, Cardiovascular response to posture changes: Multiscale modeling and in vivo validation during head-up tilt, Front. Physiol. 13 (2022) 826989.

[44] M. Fois, L. Ridolfi, S. Scarsoglio, In silico study of the posture-dependent cardiovascular performance during parabolic flights, Acta Astronaut. 200 (2022) 435–447.

[45] S. Scarsoglio, M. Fois, L. Ridolfi, Increased hemodynamic pulsatility in the cerebral microcirculation during parabolic flight-induced microgravity: A computational investigation, Acta Astronaut. 211 (2023) 344–352.

[46] M. Fois, A. Diaz-Artiles, S. Y. Zaman, L. Ridolfi, S. Scarsoglio, Linking cerebral hemodynamics and ocular microgravity-induced alterations through an in silico-in vivo head-down tilt framework, npj Microgravity 10(1) (2024) 22.

[47] M. Fois, L. Ridolfi, S. Scarsoglio, Arterial wave dynamics preservation upon orthostatic stress: a modelling perspective, Roy. Soc. Open Sci. 10(3) (2023) 221257.

[48] K. Tateno, L. Glass, Automatic detection of atrial fibrillation using the coefficient of variation and density histograms of RR and ΔRR intervals, Med. Biol. Eng. Comput. 39(6) (2001) 664–671.

[49] J. Hayano, F. Yamasaki, S. Sakata, A. Okada, S. Mukai, T. Fujinami, Spectral characteristics of ventricular response to atrial fibrillation, Am. J. Physiol. Heart C. 273(6) (1997) H2811–H2816.

[50] T. Hennig, P. Maass, J. Hayano, S. Heinrichs, Exponential distribution of long heart beat intervals during atrial fibrillation and their relevance for white noise behaviour in power spectrum, J. Biol. Phys. 32(5) (5) (2007) 383–392.

[51] R. S. Wijesurendra, B. Casadei, Atrial fibrillation: Effects beyond the atrium?, Cardiovasc. Res. 105 (3) (2015) 238–247.

[52] E. Anter, M. Jessup, D. J. Callans, Atrial fibrillation and heart failure: Treatment considerations for a dual epidemic, Circulation 119 (18) (2009) 2516–2525.

[53] M. Tanabe, K. Onishi, K. Dohi, T. Kitamura, M. Ito, T. Nobori, *et al.*, Assessment of left ventricular systolic function in patients with chronic atrial fibrillation and dilated cardiomyopathy using the ratio of preceding to prepreceding R–R intervals, Int. J. Cardiol. 108(2) (2006) 197–201.

[54] Y.-M. Cha, A. Wokhlu, S. J. Asirvatham, W.-K. Shen, P. A. Friedman, T. M. Munger, *et al.*, Success of ablation for atrial fibrillation in isolated left ventricular diastolic dysfunction: A comparison to systolic dysfunction and normal ventricular function, Circ. Arrhythmia Elec. 4(5) (2011) 724–732.

[55] P. Zhu, Y. Zhang, P. Jiang, Z. Wang, J. Wang, X. Yin, *et al.*, Effects of radiofrequency catheter ablation on left ventricular structure and function in patients with atrial fibrillation: A meta-analysis, J. Interv. Card. Electr. 40(2) (2014) 137–145.

[56] F. Haddad, S. A. Hunt, D. N. Rosenthal, D. J. Murphy, Right ventricular function in cardiovascular disease, part i: anatomy, physiology, aging, and functional assessment of the right ventricle, Circulation 117 (2008) 1436–1448.

[57] E. S. Nelson, J. G. Myers, B. E. Lewandowski, C. Ross Ethier, B. C. Samuels, Acute effects of posture on intraocular pressure, Plos One 15(2) (2020) e0226915.

[58] T. Higashide, S. Udagawa, K. Nakazawa, Y. Yamashita, S. Tsuchiya, S. Ohkubo, *et al.*, Prediction of glaucoma progression by 24-h contact lens sensor profile in patients with normal-tension glaucoma, Sci. Rep. 14 (1) (2024) 21564.

[59] S. Masai, K. Ishida, A. Anraku, T. Takumi, G. Tomita, Pulse Waveform Analysis of the Ocular Blood Flow Using Laser Speckle Flowgraphy before and after Glaucoma Treatment, J. Ophthal. 2019 (1) (2019) 1980493.

[60] T. Sugiyama, H. Nakamura, Increased Short-Term Fluctuation in Optic Nerve Head Blood Flow in a Case of Normal-Tension Glaucoma by the Use of Laser Speckle Flowgraphy, Vision 1 (1) (2016) 5.

[61] A. Vinnett, J. Kandukuri, C. Le, K.-A. Cho, A. Sinha, S. Asanad, *et al.*, Dynamic Alterations in Blood Flow in Glaucoma Measured with Laser Speckle Contrast Imaging, Ophthalmology Glaucoma 5 (3) (2022) 250–261.

[62] A. C. Guyton, J. E. Hall, Textbook of medical physiology, Elsevier Saunders Philadelphia (2011).